75, indicating that C108 is contributing but not crucial for catalysis. In contrast, mutating cysteine 265 to alanine resulted in complete loss of activity (Fig. 4C). These findings are in agreement with β-elimination demanding only one proton abstraction (as opposed to isomerization) and with C265 acting as the catalytic base.

The *E. huxleyi* genome has 7 *Alma* paralogs (see the SM) (Fig. 4A) (*16*). However, the transcriptome analysis indicates that *Alma1* is by far the most highly expressed *Alma* gene in HL*373* (≥40 times as much as all other paralogs) (Fig. 3). There appear to be four clades of *Alma* paralogs, with *Alma3/6* and *Alma7* (Clade A) being most closely related to *Alma* genes from *Phaeocystis antarctica*, another bloom-forming algal species that possesses high DMSP lyase activity and large DMS emissions (*20*, *22*). Clade A (Fig. 4A) also includes key algal species that are known to possess high DMSP lyase activity, dinoflagellates (e.g., *Symbiodinium* sp., a coral symbiont), other haptophytes (e.g., *Prymnesium parvum*) (*20*, *30*), and coral orthologs (*Acropora millepora*). Although DMSP can also be produced by corals (*31*), DMSP lyase activity is thought to be associated with symbiotic algae and/or associated bacteria and not with the coral itself (*32*). Within clade B (Fig. 4A), several *Alma* genes were found to have two Alma1-like domains fused in tandem, including *E. huxleyi Alma4/5* and the *Chrysochromulina polylepis* gene. Clade C (Fig. 4A) includes *E. huxleyi Alma1* and *Alma2* that also appear in the closely related *Isochrysis*. The more distant clade D comprises bacterial genes with ~30% identity to *Alma1*, but its relevance is yet to be determined. We synthesized five genes from across the phylogenetic tree and expressed them in *E. coli* (see the SM). Two genes, *E. huxleyi Alma2* (clade C) and *Symbiodinium*-A1 (clade A) were expressed at low levels, yet exhibited lyase activity upon feeding DMSP to *E. coli* culture (fig. S10). However, these two enzymes were not sufficiently stable to be purified.

The identification of the family members of the newly identified algal DMSP lyase in a wide range of marine organisms would enable better understanding of the physiological and signaling roles of DMS in algal resistance to viral infection, predation (*5*), and commensal (*14*) and symbiotic interaction (*31*). Although it is clear that DMS production by bacteria DMSP lyases has a fundamental role in the oceanic sulfur and carbon cycles, the newly revealed algal enzyme may allow quantification of the relative biogeochemical contribution of algae and bacteria to the global DMS production.

REFERENCES AND NOTES

1. W. Sunda, D. J. Kieber, R. P. Kiene, S. Huntsman, *Nature* **418**, 317–320 (2002).
2. E. Garcés, E. Alacid, A. Reñé, K. Petrou, R. Simó, *ISME J.* **7**, 1065–1068 (2013).
3. M. Garren *et al.*, *ISME J.* **8**, 999–1007 (2014).
4. J. Decelle *et al.*, *Proc. Natl. Acad. Sci. U.S.A.* **109**, 18000–18005 (2012).
5. G. V. Wolfe, M. Steinke, G. O. Kirst, *Nature* **387**, 894–897 (1997).
6. A. J. Kettle, M. O. Andreae, *J. Geophys. Res. Atmos.* **105** (D22), 26793–26808 (2000).
7. R. J. Charlson, J. E. Lovelock, M. O. Andreae, S. G. Warren, *Nature* **326**, 655–661 (1987).
8. P. K. Quinn, T. S. Bates, *Nature* **480**, 51–56 (2011).
9. J. R. Seymour, R. Simó, T. Ahmed, R. Stocker, *Science* **329**, 342–345 (2010).
10. M. S. Savoca, G. A. Nevitt, *Proc. Natl. Acad. Sci. U.S.A.* **111**, 4157–4161 (2014).
11. A. R. Curson, J. D. Todd, M. J. Sullivan, A. W. Johnston, *Nat. Rev. Microbiol.* **9**, 849–859 (2011).
12. C. R. Reisch, M. A. Moran, W. B. Whitman, *Front Microbiol* **2**, 172 (2011).
13. M. A. Moran, C. R. Reisch, R. P. Kiene, W. B. Whitman, *Annu. Rev. Mar. Sci.* **4**, 523–542 (2012).
14. R. Simó, *Trends Ecol. Evol.* **16**, 287–294 (2001).
15. W. M. Balch, P. M. Holligan, S. G. Ackleson, K. J. Voss, *Limnol. Oceanogr.* **36**, 629–643 (1991).
16. B. A. Read *et al.*, *Nature* **499**, 209–213 (2013).
17. M. Steinke, G. V. Wolfe, G. O. Kirst, *Mar. Ecol. Prog. Ser.* **175**, 215–225 (1998).
18. G. L. Cantoni, D. G. Anderson, *J. Biol. Chem.* **222**, 171–177 (1956).
19. M. P. de Souza, Y. P. Chen, D. C. Yoch, *Planta* **199**, 433–438 (1996).
20. J. Stefels, L. Dijkhuizen, *Mar. Ecol. Prog. Ser.* **131**, 307–313 (1996).
21. M. K. Nishiguchi, L. J. Goff, *J. Phycol.* **31**, 567–574 (1995).
22. B. R. Mohapatra, A. N. Rellinger, D. J. Kieber, R. P. Kiene, *Aquat. Biol.* **18**, 185–195 (2013).
23. J. Stefels, *J. Sea Res.* **43**, 183–197 (2000).
24. B. R. Lyon, P. A. Lee, J. M. Bennett, G. R. DiTullio, M. G. Janech, *Plant Physiol.* **157**, 1926–1941 (2011).
25. U. Alcolombri, P. Laurino, P. Lara-Astiaso, A. Vardi, D. S. Tawfik, *Biochemistry* **53**, 5473–5475 (2014).
26. J. D. Todd *et al.*, *Science* **315**, 666–669 (2007).
27. P. von Dassow *et al.*, *Genome Biol.* **10**, R114 (2009).
28. S. D. Rokitta *et al.*, *J. Phycol.* **47**, 829–838 (2011).
29. U. Alcolombri, M. Elias, A. Vardi, D. S. Tawfik, *Proc. Natl. Acad. Sci. U.S.A.* **111**, E2078–E2079 (2014).
30. A. M. N. Caruana, G. Malin, *Prog. Oceanogr.* **120**, 410–424 (2014).
31. J. B. Raina *et al.*, *Nature* **502**, 677–680 (2013).
32. J. B. Raina, E. A. Dinsdale, B. L. Willis, D. G. Bourne, *Trends Microbiol.* **18**, 101–108 (2010).

ACKNOWLEDGMENTS

We thank S. Albeck for assistance with the gel filtration analysis, S. Rosenwasser for important insights regarding the transcriptome de novo construction, U. Sheyn for assistance with the experimental setup for the transcriptome, A. Admon for mass spectrometry, P. Laurino for the nuclear magnetic resonance analysis, R. Hashayev for technical assistance with fractionation, and S. Graff for the graphic design. We gratefully acknowledge financial support from the Sasson and Marjorie Peress Philanthropic Fund to D.S.T. and from the European Research Council (ERC) StG (INFOTROPHIC grant 280991) to A.V. All data are available in the supplementary materials. Transcriptome sequences are deposited in NCBI's Sequence Read Archive, BioProjectID PRJNA283462. Author contributions: U.A., D.S.T, and A.V. conceived the project, designed the experiments, analyzed the data, and wrote the paper. U.A. performed the experiments. S.B.-D. and E.F. performed the transcriptome analyses. Y.L. performed the shotgun proteomics.

SUPPLEMENTARY MATERIALS

www.sciencemag.org/content/348/6242/1466/suppl/DC1
Materials and Methods
Figs. S1 to S10
Tables S1 to S3
References (*33*–*41*)

19 March 2015; accepted 15 May 2015
10.1126/science.aab1586

CLIMATE CHANGE

Possible artifacts of data biases in the recent global surface warming hiatus

Thomas R. Karl,[1]* Anthony Arguez,[1] Boyin Huang,[1] Jay H. Lawrimore,[1] James R. McMahon,[2] Matthew J. Menne,[1] Thomas C. Peterson,[1] Russell S. Vose,[1] Huai-Min Zhang[1]

Much study has been devoted to the possible causes of an apparent decrease in the upward trend of global surface temperatures since 1998, a phenomenon that has been dubbed the global warming "hiatus." Here, we present an updated global surface temperature analysis that reveals that global trends are higher than those reported by the Intergovernmental Panel on Climate Change, especially in recent decades, and that the central estimate for the rate of warming during the first 15 years of the 21st century is at least as great as the last half of the 20th century. These results do not support the notion of a "slowdown" in the increase of global surface temperature.

The Intergovernmental Panel on Climate Change (IPCC) Fifth Assessment Report (*1*) concluded that the global surface temperature "has shown a much smaller increasing linear trend over the past 15 years [1998–2012] than over the past 30 to 60 years." The more recent trend was "estimated to be around one-third to one-half of the trend over 1951–2012." The apparent slowdown was termed a "hiatus" and inspired a suite of physical explanations for its cause, including changes in radiative forcing, deep ocean heat uptake, and atmospheric circulation changes (*2*–*12*). Although these analyses and theories have considerable merit in helping to understand the global climate system, other important aspects of the "hiatus" related to observational biases in global surface temperature data have not received similar attention. In particular, residual data biases in the modern era could well have muted recent warming, and as stated by IPCC, the trend period itself was short and commenced with a strong El Niño

[1]National Oceanographic and Atmospheric Administration (NOAA), National Centers for Environmental Information (NCEI), Asheville, NC 28801, USA. [2]LMI, McLean, VA, USA.
*Corresponding author. E-mail: thomas.r.karl@noaa.gov

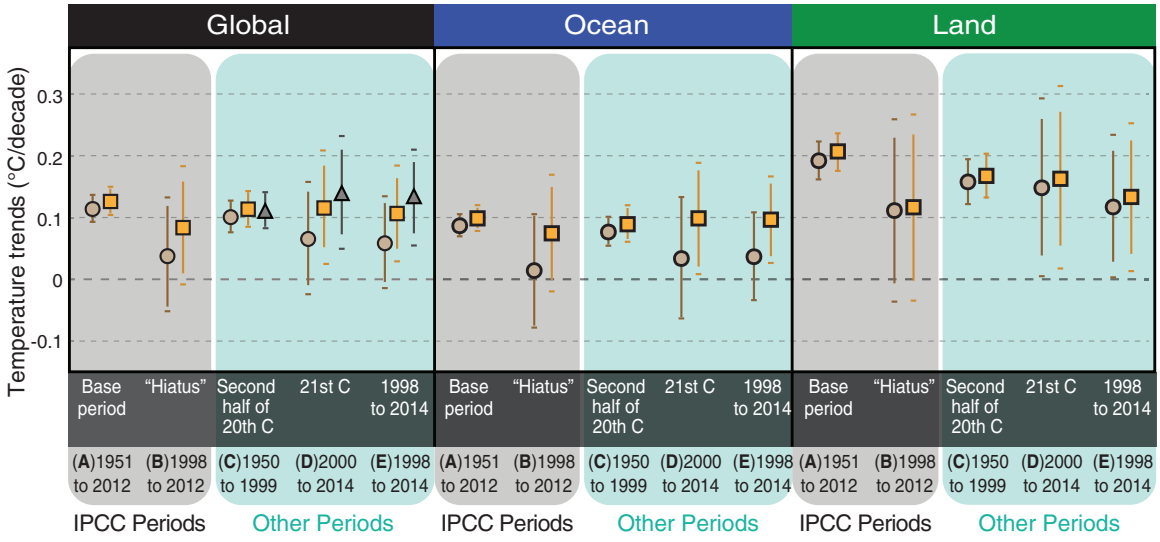

Fig. 1. Effect of new analysis on global surface temperature trends for several periods. Temperature trends are shown for data with the "new" analysis (squares) and "old" analysis (circles) for several periods of interest. Also indicated are global values calculated with the new corrections and the polar interpolation method (triangles). Consistent with the IPCC report (*1*), the error bars represent the 90% confidence intervals (CIs). The additional error associated with uncertainty of our corrections extends the 90% CI and is depicted with a horizontal dash. (**A** and **B**) The base period (1951–2012) and "hiatus" period used in IPCC (*1*). (**C**) An alternate base period, the second half of the 20th century. (**D**) The 21st century through 2014. (**E**) 1998 (a strong El Niño year) through the 21st century. Source data are provided in table S1.

in 1998. Given recent improvements in the observed record (*13*, *14*) and additional years of global data (including a record-warm 2014), we reexamine the observational evidence related to a "hiatus" in recent global surface warming.

The data used in our long-term global temperature analysis primarily involve surface air temperature observations taken at thousands of weather-observing stations over land, and for coverage across oceans, the data are sea surface temperature (SST) observations taken primarily by thousands of commercial ships and drifting surface buoys. These networks of observations are always undergoing change. Changes of particular importance include (i) an increasing amount of ocean data from buoys, which are slightly different than data from ships; (ii) an increasing amount of ship data from engine intake thermometers, which are slightly different than data from bucket seawater temperatures; and (iii) a large increase in land-station data, which enables better analysis of key regions that may be warming faster or slower than the global average. We address all three of these, none of which were included in our previous analysis used in the IPCC report (*1*).

First, several studies have examined the differences between buoy- and ship-based data, noting that the ship data are systematically warmer than the buoy data (*15*–*17*). This is particularly important because much of the sea surface is now sampled by both observing systems, and surface-drifting and moored buoys have increased the overall global coverage by up to 15% (supplementary materials). These changes have resulted in a time-dependent bias in the global SST record, and various corrections have been developed to account for the bias (*18*). Recently, a new correction (*13*) was developed and applied in the Extended Reconstructed Sea Surface Temperature (ERSST) data set version 4, which we used in our analysis. In essence, the bias correction involved

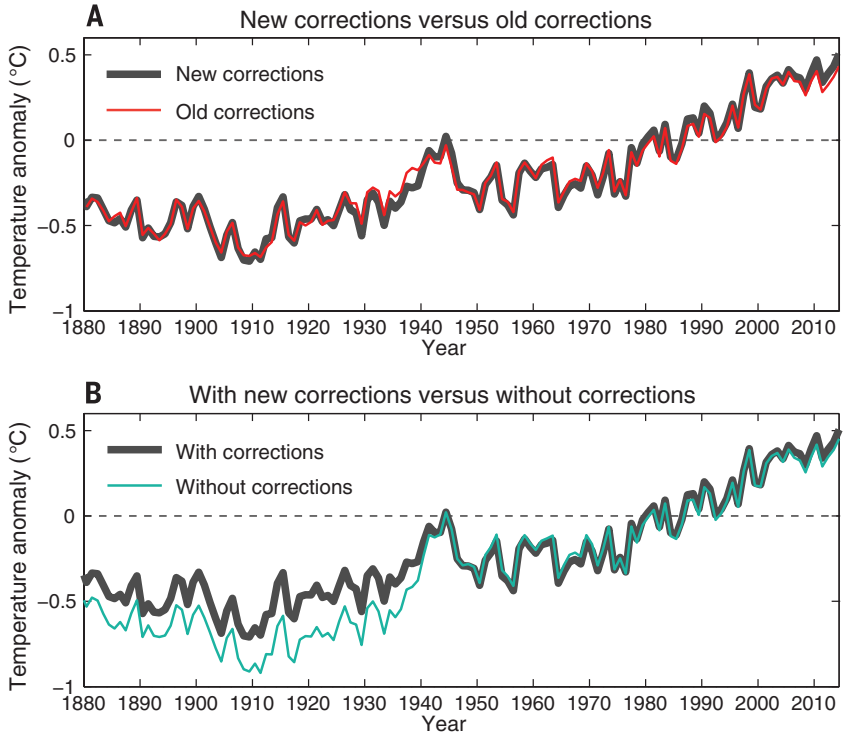

Fig. 2. Global (land and ocean) surface temperature anomaly time series with new analysis, old analysis, and with and without time-dependent bias corrections. (**A**) The new analysis (solid black) compared with the old analysis (red). (**B**) The new analysis (solid black) versus no corrections for time-dependent biases (blue).

calculating the average difference between collocated buoy and ship SSTs. The average difference globally was −0.12°C, a correction that is applied to the buoy SSTs at every grid cell in ERSST version 4. [IPCC (*1*) used a global analysis from the UK Met Office that found the same average ship-buoy difference globally, although the corrections applied in that analysis were equal to differences observed within each ocean basin (*18*).] More generally, buoy data have been proven to be more accurate and reliable than ship data, with better-known instrument characteristics and automated sampling (*16*). Therefore, ERSST version 4 also considers this smaller buoy uncertainty in the reconstruction (*13*).

Second, there was a large change in ship observations (from buckets to engine intake thermometers) that peaked around World War II. The

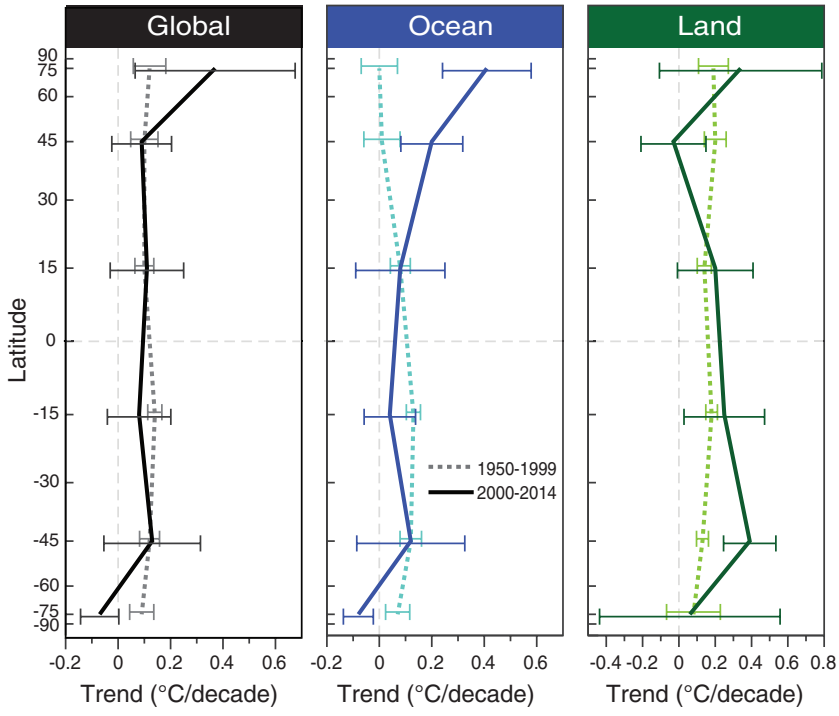

Fig. 3. Latitudinal profiles of surface temperature trends. Zonal mean trends and statistical uncertainty of the trend estimates for global, ocean, and land surface temperature, averaged in 30° latitudinal belts, for the second half of the 20th century (dashed) compared with the past 15 years (solid). Trends are cosine-weighted within latitude belts, and the vertical axis is on a sine scale so as to reflect the proportional surface area of the latitude bands. Only the uncertainty related to the trend estimates is provided because zonal standard errors of estimate are not available in contrast to the global averages.

previous version of ERSST assumed that no ship corrections were necessary after this time, but recently improved metadata (*18*) reveal that some ships continued to take bucket observations even up to the present day. Therefore, one of the improvements to ERSST version 4 is extending the ship-bias correction to the present, based on information derived from comparisons with night marine air temperatures. Of the 11 improvements in ERSST version 4 (*13*), the continuation of the ship correction had the largest impact on trends for the 2000–2014 time period, accounting for 0.030°C of the 0.064°C trend difference with version 3b. [The buoy offset correction contributed 0.014°C decade^{-1} to the difference, and the additional weight given to the buoys because of their greater accuracy contributed 0.012°C decade^{-1} (supplementary materials).]

Third, there have also been advancements in the calculation of land surface air temperatures (LSTs). The most important is the release of the International Surface Temperature Initiative (ISTI) databank (*14*, *19*), which forms the basis of the LST component of our new analysis. The ISTI databank integrates the Global Historical Climatology Network (GHCN)–Daily data set (*20*) with more than 40 other historical data sources, more than doubling the number of stations available. The resulting integration improves spatial coverage over many areas, including the Arctic, where temperatures have increased rapidly in recent decades (*1*). We applied the same methods used in our old analysis for quality control, time-dependent bias corrections, and other data processing steps (*21*) to the ISTI databank in order to address artificial shifts in the data caused by changes in, for example, station location, temperature instrumentation, observing practice, urbanization, and siting conditions. These corrections are essentially the same as those used in the GHCN–Monthly version 3 data set (*22*, *23*), which is updated operationally by the National Oceanographic and Atmospheric Administration's (NOAA's) National Centers for Environmental Information (NCEI). To obtain our new global analysis, the corrected ISTI land data (*14*) were systematically merged with ERSST version 4 (*13*), as described in the supplementary materials.

In addition to the three improvements just discussed, since the IPCC report (*1*) new analyses (*24*) have revealed that incomplete coverage over the Arctic has led to an underestimate of recent (since 1997) warming in the Hadley Centre/Climate Research Unit data used in the IPCC report (*1*). These analyses have surmised that incomplete Arctic coverage also affects the trends from our analysis as reported by IPCC (*1*). We address this issue as well.

Temperature trends in our old analysis and our new analysis are depicted in Fig. 1, supplemented with polar interpolation. (In this discussion, "old" refers to the analysis based on ERSST version 3b for ocean areas and GHCN–Monthly version 3 for land areas). For the most recent IPCC period (1998–2012), the new analysis exhibits more than twice as much warming as did the old analysis at the global scale (0.086° versus 0.039°C decade^{-1}) (table S1). This is clearly attributable to the new SST analysis, which itself has much higher trends (0.075° versus 0.014°C decade^{-1}). In contrast, trends in the new LST analysis are only slightly higher (0.117° versus 0.112°C decade^{-1}).

IPCC (*1*) acknowledged that trends since 1998 were tenuous because the period was short and commenced with a strong El Niño. Two additional years of data are now available to revisit this point, including a record-warm 2014, and trends computed through 2014 confirm the IPCC supposition. Specifically, the central trend estimate in our new analysis for 1998–2014 is 0.020°C decade^{-1} higher as compared with 1998–2012. Likewise, global trends for 2000–2014 are 0.030°C decade^{-1} higher than for 1998–2012. In other words, changing the start and end date by 2 years does in fact have a notable impact on the assessment of the rate of warming, but less compared with the impact of new time-dependent bias corrections.

Our analysis also suggests that short- and long-term warming rates are far more similar than previously estimated in IPCC's report (*1*). The difference between the trends in two periods used in IPCC's report (1998–2012 and 1951–2012) (*1*) is an illustrative metric: The trends for these two periods in the new analysis differ by 0.043°C decade^{-1} compared with 0.078°C decade^{-1} in the old analysis reported by IPCC (*1*). The smaller difference results from more warming in the new ocean analysis since 1998, reflecting the improved bias corrections in ERSST version 4. The new corrections show that the 90% confidence interval for 1998–2012 encompasses the best estimate of the trend for 1951–2012.

Also, the new global trends are statistically significant and positive at the 0.10 significance level for 1998–2012 (Fig. 1 and table S1) by using the approach described in (*25*) for determining trend uncertainty. In contrast, the IPCC report (*1*), which also used the approach in (*25*), reported no statistically significant trends for 1998–2012 in any of the three primary global surface temperature data sets. Moreover, for 1998–2014 our new global trend is 0.106° ± 0.058°C decade^{-1}, and for 2000–2014, it is 0.116° ± 0.067°C decade^{-1} (table S1). This is similar to the warming of the last half of the 20th century (Fig. 1). A more comprehensive approach for determining the 0.10 significance level (supplementary materials), which also accounts for the impact of annual errors of estimate on the trend, shows that the 1998–2014 and 2000–2014 trends (but not 1998–2012) were positive at the 0.10 significance level.

For the full period of record (1880–present) (Fig. 2), the new global analysis has essentially the same rate of warming as that of the previous analysis (0.068°C decade^{-1} and 0.065°C decade^{-1}, respectively) (table S1), reinforcing the point that the new corrections mainly have an impact in recent decades. However, it is also clear that the long-term trend would be significantly higher (0.085°C decade^{-1}) (Fig. 2B) without corrections for other historical biases, as described in (*26*).

There are important differences between the latitudinal structure of trends for the second half of the 20th century and for the 21st century (2000–2014) (Fig. 3). For example, the Arctic latitudes have shown strong warming trends both over the land and ocean since 2000, but during the latter half of the 20th century, the ocean trends in this area are near zero. The longer-term 50-year trend has more consistency in the rates of warming across all latitudes, and this is even more evident over the full period of record back to 1880 (fig. S1). There is a distinct Northern Hemisphere mid-latitude cooling in LST during the 21st century, which is also showing up in cooling of the cold extremes, as reported for the extreme minimum temperatures in this zone in (*27*). Atmospheric teleconnections and regional forcings could be relevant in understanding these short time-scale zonal trends. It is evident that in most latitude bands, the global trends in the past 15 years are comparable with trends in the preceding 50 years.

Last, we considered the impact of larger warming rates in high latitudes (*24*) on the overall global trend. To estimate the magnitude of the additional warming, we applied large-area interpolation over the poles using the limited observational data available. Results indicate that, indeed, additional global warming of a few hundredths of a degree Celsius per decade over the 21st century is evident (Fig. 1), providing further evidence against the notion of a recent warming "hiatus" (supplementary materials).

Newly corrected and updated global surface temperature data from NOAA's NCEI do not support the notion of a global warming "hiatus." As shown in Fig. 1, there is no discernable (statistical or otherwise) decrease in the rate of warming between the second half of the 20th century and the first 15 years of the 21st century. Our new analysis now shows that the trend over the period 1950–1999, a time widely agreed as having significant anthropogenic global warming (*1*), is 0.113°C decade^{-1}, which is virtually indistinguishable from the trend over the period 2000–2014 (0.116°C decade^{-1}). Even starting a trend calculation with 1998, the extremely warm El Niño year that is often used as the beginning of the "hiatus," our global temperature trend (1998–2014) is 0.106°C decade^{-1}—and we know that is an underestimate because of incomplete coverage over the Arctic. Indeed, according to our new analysis, the IPCC's (*1*) statement of 2 years ago—that the global surface temperature "has shown a much smaller increasing linear trend over the past 15 years than over the past 30 to 60 years"—is no longer valid.

REFERENCES AND NOTES

1. IPCC, *Climate Change 2013: The Physical Science Basis. Contribution of Working Group I to the Fifth Assessment Report of the Intergovernmental Panel on Climate Change*, T. F. Stocker, D. Qin, G.-K. Plattner, M. Tignor, S.K. Allen, J. Boschung, A. Nauels, Y. Xia, V. Bex, P.M. Midgley, Eds. (Cambridge Univ. Press, Cambridge, 2013).
2. G. A. Meehl, H. Teng, J. M. Arblaster, *Nature Clim. Change* **4**, 898–902 (2014).
3. G. A. Meehl, A. Hu, J. M. Arblaster, J. Fasullo, K. E. Trenberth, *J. Clim.* **26**, 7298–7310 (2013).
4. Y. Kosaka, S.-P. Xie, *Nature* **501**, 403–407 (2013).
5. M. H. England *et al.*, *Nature Clim. Change* **4**, 222–227 (2014).
6. B. D. Santer *et al.*, *Nat. Geosci.* **7**, 185–189 (2014).
7. G. A. Schmidt, D. T. Shindell, K. Tsigaridis, *Nat. Geosci.* **7**, 158–160 (2014).
8. J. Tollefson, *Nature* **505**, 276–278 (2014).
9. M. Watanabe *et al.*, *Geophys. Res. Lett.* **40**, 3175–3179 (2013).
10. J. C. Fyfe, N. P. Gillett, *Nature Clim. Change* **4**, 150–151 (2014).
11. K. E. Trenberth, J. T. Fasullo, M. A. Balmaseda, *J. Clim.* **27**, 3129–3144 (2014).
12. H. Ding, R. J. Greatbatch, M. Latif, W. Park, R. Gerdes, *J. Clim.* **26**, 7650–7661 (2013).
13. B. Huang *et al.*, *J. Clim.* **28**, 911–930 (2015).
14. J. J. Rennie *et al.*, *Geosci. Data J.* **1**, 75–102 (2014).
15. E. C. Kent, J. J. Kennedy, D. I. Berry, R. O. Smith, *Clim. Change* **1**, 718–728 (2010).
16. R. W. Reynolds, N. A. Rayner, T. M. Smith, D. C. Stokes, W. Wang, *J. Clim.* **15**, 1609–1625 (2002).
17. R. W. Reynolds, D. B. Chelton, *J. Clim.* **23**, 3545–3562 (2010).
18. J. J. Kennedy, N. A. Rayner, R. O. Smith, D. E. Parker, M. Saunby, *J. Geophys. Res. Atmos.* **116** (D14), D14104 (2011).
19. J. H. Lawrimore, J. J. Rennie, P. W. Thorne, *Eos* **94**, 61 (2014).
20. M. J. Menne, I. Durre, R. S. Vose, B. E. Gleason, T. G. Houston, *J. Atmos. Ocean. Technol.* **29**, 897–910 (2012).
21. M. J. Menne, C. N. Williams Jr., *J. Clim.* **22**, 1700–1717 (2009).
22. J. H. Lawrimore *et al.*, *J. Geophys. Res.* **116** (D19), D19121 (2011).
23. C. N. Williams, M. J. Menne, P. W. Thorne, *J. Geophys. Res.* **117** (D5), D05116 (2012).
24. K. Cowtan, R. G. Way, *Q. J. Roy. Met. Soc.* **140**, 1935–1944 (2014).
25. B. Santer *et al.*, *Int. J. Climatol.* **28**, 1703–1722 (2008).
26. T. M. Smith, R. W. Reynolds, *J. Clim.* **16**, 1495–1510 (2003).
27. J. Sillman, M. G. Donat, J. C. Fyfe, F. W. Zwiers, *Environ. Res. Lett.* **9**, 064023 (2014).

ACKNOWLEDGMENTS

We thank the many scientists at NCEI and at other institutions who routinely collect, archive, quality control, and provide access to the many complex data streams that go into the computation of the global surface temperature. In particular, we thank T. Boyer, B. Gleason, J. Matthews, J. Rennie, and C. Williams for their contributions to this analysis. We also thank J. Meehl and P. Duffy for constructive comments on an early version of this manuscript.

SUPPLEMENTARY MATERIALS

www.sciencemag.org/content/348/6242/1469/suppl/DC1
Materials and Methods
Fig. S1
Table S1
References (*28*–*38*)

23 December 2014; accepted 21 May 2015
Published online 4 June 2015;
10.1126/science.aaa5632

BRAIN CIRCUITS

A parvalbumin-positive excitatory visual pathway to trigger fear responses in mice

Congping Shang,[1,2] Zhihui Liu,[1] Zijun Chen,[1,2] Yingchao Shi,[1,2] Qian Wang,[1] Su Liu,[1] Dapeng Li,[1] Peng Cao[1]*

The fear responses to environmental threats play a fundamental role in survival. Little is known about the neural circuits specifically processing threat-relevant sensory information in the mammalian brain. We identified parvalbumin-positive (PV$^+$) excitatory projection neurons in mouse superior colliculus (SC) as a key neuronal subtype for detecting looming objects and triggering fear responses. These neurons, distributed predominantly in the superficial SC, divergently projected to different brain areas, including the parabigeminal nucleus (PBGN), an intermediate station leading to the amygdala. Activation of the PV$^+$ SC-PBGN pathway triggered fear responses, induced conditioned aversion, and caused depression-related behaviors. Approximately 20% of mice subjected to the fear-conditioning paradigm developed a generalized fear memory.

Environmental threats are detected by different sensory organs projecting to central brain areas to trigger fear responses (*1*, *2*). The superior colliculus (SC) is a retinal recipient structure (*3*, *4*) composed of different neuronal subtypes (*5*, *6*), including parvalbumin-positive (PV$^+$), somatostatin-positive (SST$^+$), and vasoactive intestinal peptide–positive (VIP$^+$) neurons (Fig. 1A and fig. S1). In addition to mediating orienting responses (*7*), the SC contributes to avoidance and defense-like behaviors (*8*–*11*). With an optogenetic approach (*12*–*14*), we found that activation of neurons expressing channelrhodopsin-2 (ChR2) in mouse SC triggered freezing that lasted 52.8 ± 5.3 s (n = 5 mice) (movie S1). This prompted us to systematically identify the key neuronal subtypes underlying this behavior.

By crossing Ai32 (*15*) with different Cre lines (Fig. 1B) (*16*, *17*), we expressed ChR2–enhanced yellow fluorescent protein (EYFP) in specific neuronal subtypes in the SC (Fig. 1C and fig. S1) and optogenetically elicited spikes in acute slices (Fig. 1D and fig. S1). Activation of SC PV$^+$ neurons, but not SST$^+$ or VIP$^+$ neurons, triggered impulsive escaping (1.18 ± 0.09 s) followed by long-lasting freezing (46.4 ± 2.8 s) (Fig. 1, E to G; fig. S1; and movie S2). To avoid activation of PV$^+$ retinal

[1]State Key Laboratory of Brain and Cognitive Sciences, Institute of Biophysics, Chinese Academy of Sciences, Beijing 100101, China. [2]University of Chinese Academy of Sciences, Beijing 100049, China.
*Corresponding author. E-mail: pcao@ibp.ac.cn

Possible artifacts of data biases in the recent global surface warming hiatus

Thomas R. Karl *et al.*

Science **348**, 1469 (2015);
DOI: 10.1126/science.aaa5632